JOURNAL OF Materials CHEMISTRY

Chemical sensors of monocyclic aromatic hydrocarbons based on sol–gel materials: synthesis, structural characterization and molecular interactions

Maria-Luisa Calvo-Muñoz,[a] Cécile Roux,[b] Francine Brunet,[c] Jean-Philippe Bourgoin,[c] André Ayral,[d] Abdeslam El-Mansouri[d] and Thu-Hoa Tran-Thi*[a]

[a]*DSM/DRECAM/SPAM/Laboratoire Francis Perrin, FRE 2298 CNRS, CEA/Saclay, 91191 Gif-sur-Yvette, Cedex, France. E-mail: tranthi@drecam.cea.fr; Fax: (33) 1 69 08 87 07; Tel: (33) 1 69 08 49 33*
[b]*Laboratoire de Chimie de la Matière Condensée, Université Paris VI, 4 place Jussieu, 75252 Paris, Cedex 05, France*
[c]*DSM/DRECAM/SCM, CEA/Saclay, 91191 Gif-sur-Yvette, Cedex, France*
[d]*ENSCM, UMII, CNRS UMR 5635, Institut Européen des Membranes, Place Eugène Bataillon, Case Courrier 047 F-34095 Montpellier Cedex, France*

Received 4th July 2001, Accepted 3rd December 2001
First published as an Advance Article on the web 24th January 2002

Low cost materials based on hybrid organic–inorganic sol–gel systems have been developed for use in the trapping and detection of monocyclic aromatic hydrocarbon contaminants emitted into the atmosphere. To this end, two strategies are followed; the first one aims at tailoring the pore size in order to selectively trap and discriminate benzene and toluene. The second is to decrease the pore polarity in order to eliminate the main interfering gas of the atmosphere, water vapor. The results of these strategies are reported in this paper. After describing the synthesis of silicon hybrid xerogels and thin films and the characterisation of their structural properties, we report the study of the local polarity of the pores, of the porosity and optical properties of the materials. These characterisation data will enable us to define the materials suited for hosting benzene and toluene.

1 Introduction

Porous materials obtained *via* the sol–gel process from alkoxysilane precursors ($Si(OR)_4$) have often been used to encapsulate dye molecules for various applications such as solid dye lasers,[1,2] electro-optical material for information storage[3,4] as well as chemical[5,6] and biochemical[7,8] sensors. This process allows the fabrication at room temperature of porous materials with high specific surface areas. The use of modified alkoxysilane precursors ($R'_xSi(OR)_{4-x}$) such as methyltrimethoxysilane easily leads to silica-based hybrid materials containing Si–O and Si–C bonds.[9,10] By varying the ratio of methyltrimethoxysilane (MeTMOS) to tetramethoxysilane (TMOS), the microstructure and the polarity of the sol–gel materials can be adjusted to trap the desired molecules. In the present work, two objectives are pursued; the first one is to tailor the pore size of the materials in order to trap air pollutants such as benzene, toluene and xylenes. The second one consists in decreasing the local polarity of the pores to eliminate one of the most important interference gases, water vapor. Thus, combining such a sensitive layer with a simple optical transduction method yields a sensor which can operate at room temperature.

In this initial work, we first describe the synthesis and structural characterisation of the monoliths and thin films of inorganic and hybrid organic–inorganic polymers. We report the study of the porosity of the materials through the analysis of their adsorption–desorption isotherms and the exploration of the local polarity of the host pores *via* various methods including near IR spectroscopy and fluorescence studies of pyranine, a molecular probe sensitive to changes of the microscopic environment. We will conclude with the choice of the best material to be used for the trapping of the air contaminants. We will show in a coming paper that, with the strategies aimed at tailoring both the size and the polarity of the pore, we are able to optimize the trapping of the pollutants and to detect 100 ppb of benzene.

2 Experimental

2.1. Chemicals

All chemicals are of analytical grade and are used without further purification. Silicon alkoxide precursors, tetramethoxysilane (TMOS) and methyltrimethoxysilane (MeTMOS) are from Aldrich. Ethanol (EtOH) of UVASOL grade is from Merck and 8-hydroxy-1,3,6-trisulfonated pyrene 99.8% pure (pyranine or 3sPyOH) was purchased from Acros Organics. Water was purified with the Milli-ro 5+ and Milli-Q systems of Millipore to a resistivity of 18.2 $M\Omega.cm^{-1}$.

2.2. Methods

Synthesis of monoliths and thin films. TMOS monoliths are prepared from a TMOS–H_2O–EtOH mixture in a one-step process. Typically, monoliths are obtained from a sol mixture containing 2.5 ml of TMOS, 1.1 ml of freshly purified water and 3.7 ml of EtOH. The molar ratio of TMOS : H_2O : EtOH, 1 : 4 : 4, allows a nearly complete hydrolysis of the O-CH_3 groups.[11,12] After 10 minutes of sonication, the sol is poured into a 40 × 10 × 4 mm polystyrene cuvette (approximately 1.6 ml per cuvette) which is then sealed with Parafilm and left to undergo gelation at room temperature for 3 days. After these 3 days, the gel has formed and three thin pinholes are punctured in the Parafilm to allow the remaining solvents, EtOH, H_2O, and MeOH formed during the polymerisation process, to slowly evaporate. The cuvettes are stored in an oven

and kept at room temperature. This drying process lasts two months during which the gel shrinks and reaches its final dimensions of 20 × 5 × 2 mm. When needed, probe molecules such as pyranine dissolved in EtOH are introduced in the starting sol, with typical concentration of 5×10^{-5} M in the final sol. The cost of such prepared monoliths with final dimensions of 20 × 5 × 2 mm, including the prices of chemicals, of ultra-pure water and of disposable cuvettes, is 0.1 Euro unit^{-1}.

Thin films are prepared with the spin-coating technique. Aging the sol for 18 hours is necessary to adjust the viscosity for a suitable coating. A few drops of the sol mixture are then spread on a quartz substrate which is spun at 4000 rpm for 30 seconds. The films are then dried on a heating hot plate maintained at 100 °C during 20 minutes.

For hybrid MeTMOS–TMOS thin films and monoliths, the same procedure is used to mix TMOS, EtOH and water. The sol mixture is then left to age during 1 hour, after which the MeTMOS is added. This protocol is based on the relative rate of hydrolysis of the two precursors, the faster being MeTMOS.[13–15] The different hybrid materials synthesized have a TMOS : MeTMOS molar ratio of 9 : 1, 8 : 2, 7 : 3 or 5 : 5. For thin films, the total cost is higher (5.8 Euro unit^{-1}) than for a monolith due to the price of the quartz substrate (dimensions: 15 × 10 × 1 mm). However, the quartz substrate is recyclable.

Solid state NMR. Solid state magic angle spinning (MAS) NMR measurements were performed with the AVANCE 500 WB (11 Tesla) spectrometer operating at 499.14 MHz for ^{1}H, at 99.15 MHz for ^{29}Si and at 125.5 MHz for ^{13}C. Solid samples were introduced in a 4 mm ZrO_2 rotor and spun at the magic angle with a spinning rate of 4 kHz for the ^{29}Si and 12 kHz for the ^{1}H and ^{13}C. For the ^{29}Si simple-pulse experiments (SPE), the pulse width (4.3 μs) and the relaxation delay (120 s) were chosen to take into account the long T_1 relaxation times. For the ^{1}H simple-pulse experiments, the pulse width was 2 μs and the relaxation delay 2 s. For the ^{13}C simple-pulse experiments, the pulse width was 2.8 μs and the relaxation delay 180 s. Tetramethylsilane (TMS) was used as the reference. The spectra were analysed with the WINNMR program.

Film thickness and surface roughness. Optical interferometry and Atomic Force Microscopy (AFM) were used to measure the film thickness. The film thickness was measured as follows. A dull tungsten tip was first used to make a scratch in the film. Then an AFM image of that scratch was recorded. The thickness of the film was then deduced from a height profile corresponding to a cross-section of that image. A film thickness of 750 ± 50 nm was obtained. In addition, AFM technique provides further information on the texture and roughness of the film. The AFM apparatus is a Nanoscope IIIa (Digital Instruments), equipped with a scanner capable of scanning a region of 16.8 × 16.8 μm^2 for the roughness measurements and texture imaging and a scanner capable of scanning 140 × 140 μm^2 for the thickness measurements. Experiments were done in air at room temperature. The images were recorded in tapping mode using a 125 μm long silicon cantilever (rectangular shape, 23 mN m^{-1} < k < 65 mN m^{-1}, Nanoprobe Gmbh).

UV, visible and near IR spectroscopy. The UV, visible and near-infrared spectra of the monoliths were measured over the 4000 to 52630 cm^{-1} range (2500 to 190 nm) with a Perkin-Elmer Lambda 900 spectrometer. The samples were dried and stored at room temperature. To eliminate the remaining interstitial water molecules, the samples were degassed under vacuum (1.33 10^{-2} Pa) and kept as such in an optical quartz cell. The optical pathlength corresponds to the thickness of the monolith or of the thin film.

Fluorimetry. Fluorescence spectra were recorded in a front face configuration with a SPEX-Fluorolog spectrofluorometer over the UV–visible domain. The excitation source is a 450 W XBO Xenon lamp. The spectra were corrected for the monochromator and photomultiplier response over the 250–750 nm range. The absorbance of the fluorescing probe is kept low enough (<0.1) to avoid spectral distortions due to the inner-filter effect and emission re-absorption.

Surface area and pore size measurements. The monoliths (0.02 g) were ground to a powder and degassed under vacuum for 24 hours at 50 °C. Adsorption–desorption isotherms of the xerogel were then recorded at 77 K with a Micrometrics ASAP 2010 volumetric analyser using N_2 as adsorptive. The surface area and pore diameter were deduced from these measurements using the Brunauer–Emmet–Teller[16] (BET) and micropore analysis (MP)[17] methods. Micropore area was determined by the *t*-plot method.[18]

For thin films, we adopted the procedure developed by Ayral *et al.*[19] for sol–gel coatings on glass substrates. The substrates (76 × 26 × 1 mm) are individually weighed and then coated. The coated slides are dried at room temperature for several hours and then heated to 100 °C. The slides, still warm, are weighed in order to avoid adsorption of atmospheric water. Fifteen slides are needed to get the amount of matter necessary (0.02 g) for the adsorption–desorption experiment. They are introduced into a glass cell which is sealed and then connected to the adsorption apparatus. The adsorption–desorption isotherms of nitrogen were then recorded at 77 K with a Micrometrics ASAP 2000 apparatus.

3 Results and discussion

It is well known that the final properties of sol–gel materials are very dependent not only on the parameters which govern the kinetics of the hydrolysis and condensation processes[20] but also on the drying stage. These problems were clearly addressed in the past by the group of Phalippou.[21] Thus, it is important to precisely characterise the structure and texture of the xerogels.

3.1. Probing the structure of the matrices

^{29}Si MAS solid-state NMR can provide direct information on the local environment of the different structural units,[22] and thus on the degree of condensation of the network. Fig. 1 displays the ^{29}Si MAS-NMR spectra recorded for monoliths, using single-pulse experiments (SPE). We use the notation commonly adopted, Q^n and T^n units,[22] to describe the bonding environment of the silicon nucleus (see Fig. 1). In this notation, Q^n and T^n are the tetrafunctional and trifunctional sites, respectively, with n being the number of siloxane bridges around the Si atoms. For the TMOS derived xerogel, the signals between −90 and −120 ppm are due to silicon nuclei of type Q^2, Q^3 and Q^4; Q^4 and Q^3 being the most abundant species (90%) (see Table 1). For the hybrid xerogels, two regions can be distinguished in the NMR spectra around ∼−60 and ∼−110 ppm, which correspond to T^n and Q^n units, respectively. As the amount of methyl groups increases, the peaks between −50 and −70 ppm grows in intensity. In addition, Q^4 and Q^3 species decrease in favour of the linear species Q^2 and T^2. Increasing the amount of methyl groups affects the structure of the polymer in reducing the branching ratio of the network. The methyl-enriched polymer becomes more flexible.

Another important parameter is the degree of condensation, c, defined[20,23] as:

$$c = \Sigma i q_i / f$$

with q_i being the relative concentration of each silicon site

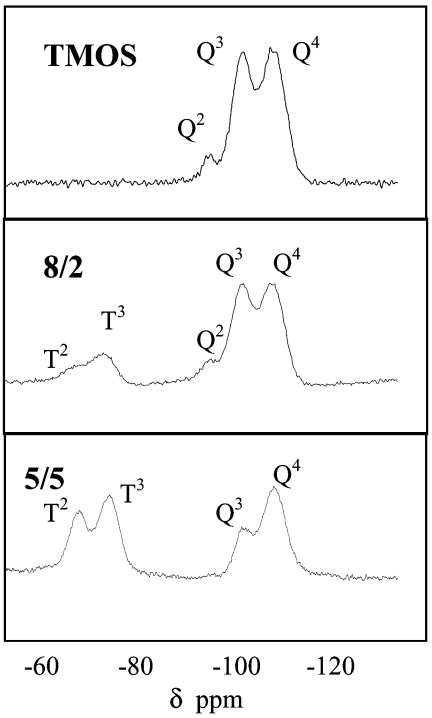

Fig. 1 ^{29}Si MAS-NMR spectra of TMOS and hybrid TMOS–MeTMOS 8 : 2 and 5 : 5 samples.

Table 1 ^{29}Si NMR-MAS data for three xerogels, TMOS and TMOS–MeTMOS 8 : 2 and 5 : 5. δ is the chemical shift referenced to TMS, q_i the percentage of the Q^n or T^n site, n being the number of bridging oxygens and c, the degree of condensation of the polymer network. X = H or R

Sample	δ/ppm	Site	Assignment	q_i (%)	c
TMOS	−91.2	Q^2	$Si(OSi)_2(OX)_2$	10	0.85
	−101.0	Q^3	$Si(OSi)_3(OX)$	43	
	−110.0	Q^4	$Si(OSi)_4$	47	
8 : 2	−54.7	T^2	CH_3–$Si(OSi)_2(OX)$	6	0.84
	−62.7	T^3	CH_3–$Si(OSi)_3$	11	
	−92.2	Q^2	$Si(OSi)_2(OX)_2$	9	
	−101.3	Q^3	$Si(OSi)_3(OX)$	37	
	−110.0	Q^4	$Si(OSi)_4$	37	
5 : 5	−55.8	T^2	CH_3–$Si(OSi)_2(OX)$	21	0.88
	−64.0	T^3	CH_3–$Si(OSi)_3$	29	
	−102.0	Q^3	$Si(OSi)_3(OX)$	16	
	−110.0	Q^4	$Si(OSi)_4$	33	

derived from the NMR spectra, i the number of oxo bridges and f the connectivity of the monomer ($f = 3$ for MeTMOS and $f = 4$ for TMOS).

Values of c are high, 0.85–0.88 (see Table 1), for all the xerogels and do not significantly change when the amount of methyl group increases. They are consistent with the ones reported by Diré *et al.*[24] for similar hybrid systems prepared from tetraethoxysilane and methyltriethoxysilane precursors. These results indicate that the amount of residual Si–OMe should be low.

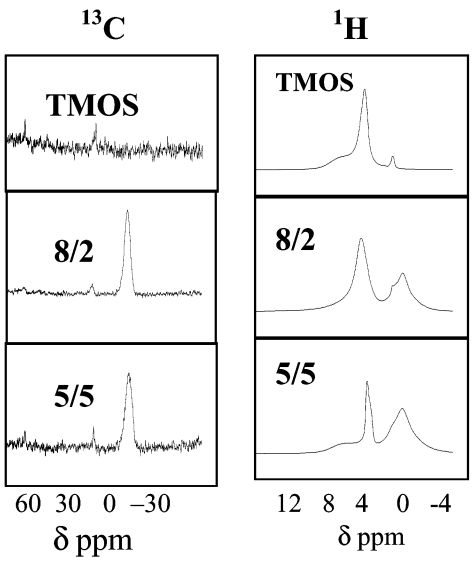

Fig. 2 ^{13}C and ^{1}H MAS-NMR spectra of TMOS and hybrid TMOS–MeTMOS 8 : 2 and 5 : 5 samples.

The ^{13}C and ^{1}H MAS NMR spectra can provide further and complementary information on the presence of the residual Si–OMe and Si–OH groups.[24,25] For instance, from the values of the chemical shift recorded in the ^{1}H NMR-MAS spectra, it is possible to discriminate the CH_3 of an –Si–CH_3[25,26] from that of CH_3–O–Si or CH_3–CH_2–O–Si[24,27,28] (see Fig. 2a and Table 2); thus, the resonance line at 1.03 ppm, attributed to the CH_3 of the ethoxy group, indicates the presence of residual Si–OEt groups. These ethoxy groups could be attributed to the non hydrolysed Si–OEt groups, coming from the transesterification and/or esterification reactions:[29,30]

$$\equiv Si–OMe + EtOH \leftrightarrow \equiv Si–OEt + MeOH$$

$$\equiv Si–OH + EtOH \leftrightarrow \equiv Si–OEt + H_2O$$

No signal at 2 ppm, which could be attributed to the free Si–O–H groups,[31,32] was observed. On the contrary, the wide resonance line covering the 4–6 ppm domain is indicative of the presence of both Si–OH groups H-bonded to water molecules and physisorbed water molecules linked to themselves.[31,32] These findings will be confirmed with the studies of the pore polarity.

For the hybrid xerogels, the ^{13}C MAS NMR spectra display signals at $\delta = -4.4$ and -5.8 ppm for the 5 : 5 and 8 : 2 xerogels, respectively (see Table 2 and Fig. 2). These signals, which are not present for the TMOS sample, are attributed to the Si–CH_3 groups in the hybrid xerogels.[24,25]

Table 2 Assignments of the ^{1}H and ^{13}C MAS-NMR observed signals and comparison with the literature data.

	^{1}H NMR		^{13}C-NMR	
Assignment	δ/ppm this work	δ/ppm literature	δ/ppm this work	δ/ppm literature
CH_3–CH_2–O–	1.03–1.15	1.3[27]	15.1–17.3	17.6–18.4[24]
CH_3–*CH_2*–O–	3.70–4.30	3.7–3.9[28]	58.8–59.5	58.1–59.9[24]
CH_3–O–				51.7[25]
CH_3–Si	0.10–0.15	0[26]–0.4[24]	−4.4 to −5.8	−2.46[25] to −3.7[24]
Isolated Si–OH	—	1.7–2[31,32]		
H-bonded Si–OH	6.5	3–8[32]		
Physisorbed H_2O	3.7–4.3	3.5[31,32]		

3.2. Probing the surface texture of thin films and monoliths

The AFM investigation of the surface of a 8 : 2 thin film (see Figs. 3a and 3b) yields the following information: the surface of the film appears very flat on a local scale (Fig. 3a). More precisely, the surface is made of small grains (of average size 9 ± 2 nm) and the RMS roughness is 4 ± 1 nm. At some places, holes a few tens of nanometres deep and 50 nm wide typically are found.

At a larger scale (Fig. 3b), the film thickness appears homogeneous with some fluctuations on a tens of micron scale: indeed, a texture shows up, made of domains a few microns wide separated by valleys about 3 ± 1 nm deep. It should be noted that the small-scale grainy texture is observed both in the domains and in the valleys.

The analysis of the 8 : 2 monolith (see Figs. 3c and 3d) is more complex with the presence of residual solvent molecules in the pores. The grains are three times bigger than those found for the thin film and the RMS roughness is 2.5 times more important (11 ± 1 nm). At a larger scale, the monolith appears as wide domains (15 μm) separated by valleys about 10 to 15 nm deep.

The difference of roughness and grain size between the thin film and monolith can be explained in terms of the synthesis method. The gelification of the thin film occurs within a few seconds while several days is needed for the monolith. The grains obtained are then smaller in the thin film than in the monolith.

3.3. Probing the pore polarity

Two methods were used to probe the polarity of the pore surface and the presence of residual water molecules which could interfere with the pollutants in the air sampling process. The first one make use of vibrational spectroscopy whose detailed assignments are available in the literature for organosilicon compounds.[24,33–38] In the second method, pyranine, a highly fluorescing compound whose excited state is very sensitive to the microenvironment, is used to probe the local polarity changes *via* its interaction with the pore surface and with interstitial water.[39–43]

3.3.1. Near IR vibrational spectroscopy. Vibrational spectroscopy in the near infrared is one of the tools well suited to probe, at a molecular level, the pore polarity as it can provide a clear distinction between the OH vibration of a silanol group and that of water. Fig. 4a displays the absorption spectra of TMOS and hybrid TMOS–MeTMOS monoliths stored for two months at room temperature and Table 3 gives the assignments of the bands.[34–38]

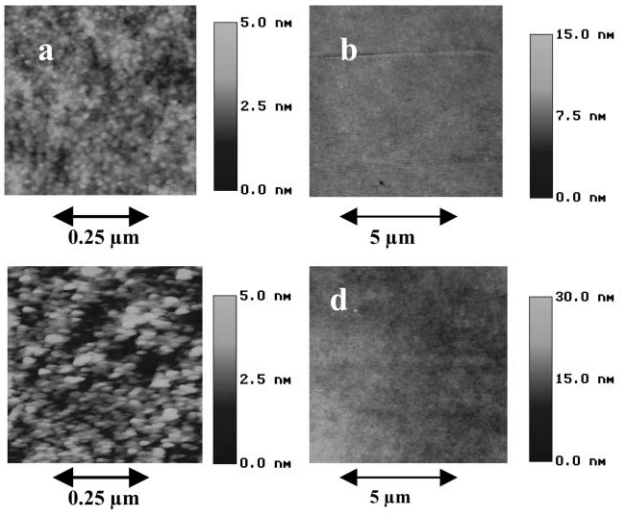

Fig. 3 Texture of a thin film (a and b) and a monolith (c and d) of TMOS–MeTMOS 8 : 2 observed with the AFM technique. (a) and (c): on a local scale, (b) and (d) on a larger scale.

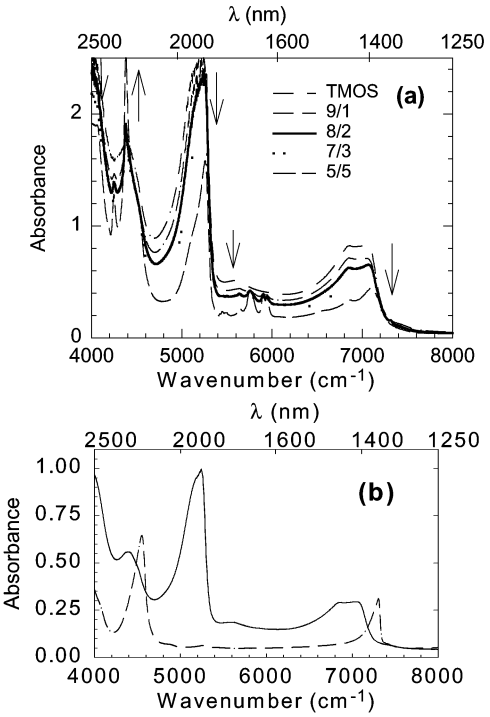

Fig. 4 Near IR spectra of (a) TMOS and hybrid xerogels stored for two months at room temperature. (b) a TMOS xerogel (thickness = 580 μm) hydrated and dehydrated under vacuum.

In all xerogels, the presence of the intense band at ~1900 nm clearly indicates the presence of interstitial water molecules linked together.[36–38] In agreement with the NMR data, the presence of free OH groups is not detected. On the contrary, the two bands peaking at ~2200 and ~1400 nm are indicative of the presence of the SiOH groups H-bonded to water molecules.[34,38] However, increasing the proportion of MeTMOS in the hybrid xerogels allows the amount of water to be decreased significantly. This phenomenon can be attributed to the water repelling effect of the hydrophobic CH_3 groups which contribute to lower the polarity of the pore surface. The remaining water molecules can be eliminated either by pumping the xerogel under vacuum or by flushing it with a dry N_2 stream at low flux (50 ml min^{-1}) for 30 minutes. The absorption spectrum of a dehydrated TMOS xerogel is shown in Fig. 4b. It can be seen that water molecules have completely vanished; the two sharp bands peaking at 1369 nm

Table 3 Assignments of the near IR absorbances collected for the samples of TMOS and TMOS–MeTMOS

TMOS		TMOS–MeTMOS		
λ/nm	ν/cm^{-1}	λ/nm	ν/cm^{-1}	Assignment[33–38]
1369	7304	1379	7252	$2\nu_{OH}$ free Si–OH
1419	7047	1409	7097	$2\nu_{OH}$ H-bonded Si–OH
1450	6896	1455	6873	$2\nu_{OH}$ H-bonded water
—	—	1683	5941	
—	—	1694	5903	$2\nu_{C-H}$ Si–CH_3
—	—	1737	5757	
1900	5263	1900	5263	$\delta_{HOH} + \nu_{OH}$ water
2197	4552	2212	4521	$\delta + \nu$ free Si–OH
2272	4401	—	—	$\nu_{Si-H} + \nu_{Si-O}$
—	—	2283	4380	$\delta_{CH3} + \nu_{C-H}$ CH_3
—	—	2356	4244	

(7304 cm^{-1}) and 2197 nm (4552 cm^{-1}), assigned to the first overtone (2 ν) of the stretching vibration of the free SiO–H and to the combination of the stretching and deformation vibrations of the free SiO–H[34,38] respectively, witness the presence of the free SiOH groups.

3.3.2. Probing the polarity with pyranine. The vibrational spectroscopy findings are corroborated with the fluorescence study of sol–gel matrices doped with a fluorescent probe molecule, pyranine, which displays the following properties. Pyranine (3sPyOH), a photoacid, becomes 10 million times more acidic in the excited state than in the ground state, but only in water or water rich media.[39,40] The excited state proton transfer leading to the corresponding fluorescing anion ($3sPyO^-$) was used in the past to probe the content of remaining water molecules during the drying process of the xerogels.[41] In organic solvents, the fluorescent species is the acid form; in these solvents, the shape of the corresponding fluorescence band and its maximum position change with the polarity, the H-bond donating and H-bond accepting character of the solvent: a blue shift of the maximum is observed when the polarity decreases and when the H-bonding character in both cases becomes weak.[40] We take advantage of these properties to probe both the pore polarity of the TMOS and hybrid MeTMOS–TMOS gels and the water content in these materials.

Fig. 5a displays the spectral evolution of the pyranine fluorescence in a thin film of TMOS, freshly prepared, dried during 2 days at room temperature and dehydrated under vacuum. The initial fluorescence band observed for the freshly prepared sample displays two peaks at 445 and 515 nm, characteristic of the maxima of the fluorescence bands of the protonated 3sPyOH* (440 nm) and deprotonated $3sPyO^-$* (512 nm) in liquid water,[39,40] respectively. When water is removed (dried sample), the deprotonated species disappears in favour of the protonated one. Further removal of the residual water by pumping the sample under vacuum results in a blue shift of the fluorescence band. At that stage, the position of the fluorescence band maximum of 3sPyOH* corresponds to the one observed in alcohol–water mixtures with mole fraction of water less than 0.2.[39,40] This is due to the fact that the pore surface is now mainly covered with Si–OH groups which interact with pyranine similarly to liquid EtOH.

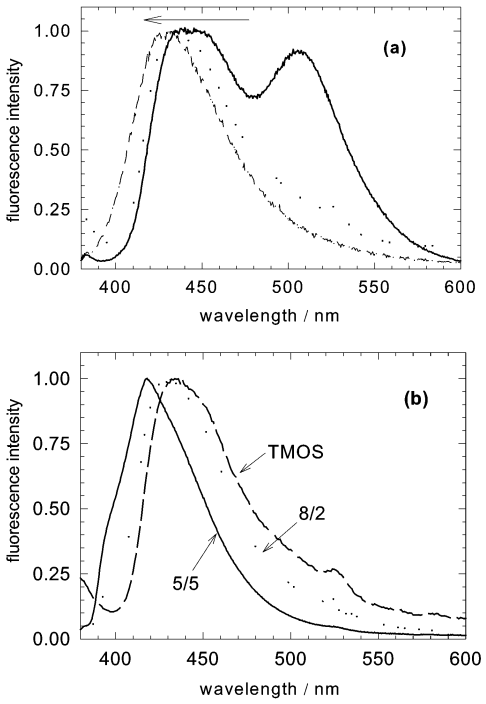

Fig. 5 Fluorescence spectrum of pyranine encapsulated in (a) a thin film of TMOS, from right to left: freshly prepared, dried for three days at room temperature, dehydrated under vacuum. (b) in various thin films of TMOS and hybrid 8 : 2 and 5 : 5 TMOS–MeTMOS.

We now compare the interactions of pyranine with the pore surface when methyl groups are added. In Fig. 5b are collected the fluorescence spectra of pyranine in a TMOS and two hybrid TMOS–MeTMOS thin films. Addition of Me groups clearly induces a blue shift of the pyranine fluorescence band. The position of the fluorescence maximum observed for the 8 : 2 film now corresponds to the one collected for pyranine in pure ethanol. It witnesses the disappearance of water, as was also demonstrated with the near IR spectrum of the dried xerogel (only shown for TMOS, see Fig. 4b). This blue shift becomes more important with increasing amount of methyl groups. It is noteworthy that such an important shift, in particular for the 5 : 5 hybrid sample (λ_{max} = 417 nm), has never been observed in the past in organic solvents. Such blue fluorescence could not be obtained as pyranine is not soluble in weakly polar solvents, such as linear hydrocarbons. In the present case, in the hybrid 5 : 5 matrix, the pore surface is now mainly covered with hydrophobic $Si–CH_3$ groups which significantly decrease the polarity of the pore.

Similar results were obtained by Wittouck *et al.*[42] when probing the polarity of hybrid TEOS and MeTEOS thin films. They also found a blue shift of the fluorescence band on adding increasing amount of MeTEOS. However, in contrast to our assignments, these authors attributed the green fluorescence to the deprotonated pyranine in the neighbourhood of the silanol groups. Our data on fluorescence, combined with those obtained with vibrational spectroscopy, clearly indicate that i) the green species (515 nm) corresponds to the deprotonated species stabilized by water molecules in water rich media; ii) this species disappears to the benefit of a blue fluorescence peaking at 425 nm in totally dehydrated samples which corresponds to the acid form of pyranine surrounded with silanols groups and iii) the blue shift increases on providing to the acid form a less polar environment enriched with methyl groups.

The results of vibrational spectroscopy and fluorescence study are consistent one with another in demonstrating the possibility of decreasing the polarity of the host cavities. Such hydrophobic media should favor the trapping of non polar pollutants, such as benzene and toluene.

3.4. Probing the porosity of thin films and monoliths

The porosity properties of organosilicon sol–gel materials are typically deduced from nitrogen adsorption–desorption isotherms. The isotherms established for all monoliths and thin films are of type I, typical of microporous solids.[18] The BET surface area, the surface area of micropores and the total pore volume of the different samples are reported in Table 4. The micropore area of xerogels is ~90% of the BET surface area,

Table 4 Porosity characteristics of monoliths and thin films of TMOS and various hybrid TMOS–MeTMOS. The doped samples contain pyranine whose concentration in the starting sol is given in parentheses

Sample	Thickness/ mm	BET surface area/$m^2\ g^{-1}$	Micropore surface area/$m^2\ g^{-1}$	Total pore volume/ $cm^3\ g^{-1}$
TMOS	2	593	579	0.304
TMOS doped (7×10^{-6} M)	2	575	553	0.301
TMOS doped (5×10^{-5} M)	2	465	460	0.260
TMOS	0.75×10^{-3}	250		0.122
9 : 1	2	645	635	0.325
8 : 2	2	623	614	0.321
5 : 5	2	100	59	—

confirming that all the monoliths are highly microporous (pore diameter <20 Å). As the amount of methyl groups in the network is increased from 0 to 10%, a very small increase of the porosity is first observed. However, further addition of methyl groups induces a decrease of the porosity. These changes could be interpreted at a first sight as a variation of the surface area around an averaged value of 610 ± 30 m^2 g^{-1}. However, the plot of the cumulative pore volume as a function of the pore radius also indicates some change: as the amount of MeTMOS increases, the small pores become less accessible and the distribution of the pore size shifts to higher values. We will see in a coming paper that this tiny increase and then decrease of the porosity can affect the efficiency of the trapping of the pollutant. With larger amounts of methyl groups, *i.e.* 50%, the value of the surface area dramatically drops (~ 100 m^2 g^{-1}). A similar behaviour was previously reported by Fahrenholtz *et al.*[43] for base catalysed silica gels prepared from mixtures of TEOS and MeTEOS. These authors found that addition of small amounts of MeTEOS below 20% to TEOS induces a small increase of the surface area, but further addition results in a significant decrease of the surface area which becomes equal to zero for 70% of MeTEOS. They attributed this loss to a collapse of the pores during the drying stage because of the weakening of the network. In our case, the very low value of the surface area of the 5 : 5 xerogel is correlated with a non coincidence of the adsorption and desorption branch of the isotherm, a behaviour which was in the past noted by Avnir and coworkers[44] for acid-catalysed microporous xerogels of TMOS. They demonstrated that the difference between the two branches stems from the slow kinetics of adsorption of N_2, giving rise to an apparent low surface area in the case of microporous materials. The observed low surface area of our 5 : 5 xerogel might be a consequence of an artefact due to a lowering of the diffusion of the N_2 into the methyl rich materials and not to a different pore structure. These data are also confirmed by another study of Krause *et al.*[45] on the *n*-hexane diffusion in mixed TMOS–MeTMOS matrices. These authors have measured with pulsed field gradient NMR techniques the diffusion coefficient of *n*-hexane in various matrices and shown that the value of the diffusion coefficient passes through a maximum for a 9 : 1 matrix and then drops with increasing amount of MeTMOS.[45] Another point to be noted is the more substantial decrease of the surface area when the sample is doped with a probe molecule, pyranine. As the presence of pyranine does not affect the pH of the starting sol (pK_a of pyranine in the ground state being equal to 7.5), the decrease of the surface area is not due to the synthesis. It is interpreted in terms of the volume occupied by pyranine adsorbed on the surface of the pores.

To determine the pore size distribution, we use the analytical MP method proposed by Mikhail *et al.*[46] Fig. 6 displays the cumulative pore volume as a function of the pore size distribution for the monolith and thin film of TMOS. Three important points can be noted. First, the cumulative pore volume reaches a plateau for low values of the pore size in the case of the thin film in contrast to the monolith for which the distribution of the pore size is wider. Second, the value of the cumulative pore volume at the plateau is two times as high for the monolith as for the thin film. Third, in the doped sample, the contribution of the smallest micropores strongly decreases and the pores with hydraulic radius higher than 4 Å are the main contributers to the total adsorbed volume.

These results indicate that the monoliths exhibit a higher porosity than their thin film analogues. Furthermore, doping the sample results in a decrease of the accessibility of the gas to the small pores because of the volume occupied by the probe molecules. The difference of properties between the thin films and monoliths will also appear in their trapping property towards benzene and toluene, as will be described in a coming work.

3.5. Probing the optical properties

The optical properties of the xerogels and thin films are important parameters to take into account when the transduction mode of the sensor is optical. Fig. 7 displays the absorption of various matrices as a function of their thickness. For thin films whose thickness varies between 660 and 750 nm, the absorbance corresponding to the matrix is negligible over UV–visible domain (not shown). For monoliths which are 200 to 3000 times thicker, the absorbance of the xerogels in the near UV is important but the materials are transparent in the visible region. We will show in a coming paper that the pollutants trapped in these matrices can be detected directly *via* their absorbance in the near UV.

4 Conclusion

In the present work, we have synthesized hybrid TMOS and MeTMOS xerogels having in mind the idea of using these porous materials to trap air pollutants such as benzene and its methylated analogs. The sol–gel method provides an easy way to process at low cost (0.1–5.8 Euros) monoliths of various size and thin films. With the vibrational spectroscopy and fluorescence analyses, we demonstrated that it is possible to decrease the polarity of the host cavities. Such hydrophobic media should favor the trapping of non polar pollutants such as benzene and toluene. The monoliths display a high porosity, three times as high as their thin films analogues, but exhibit a near UV absorption which could become important as their thickness is increased. These two parameters are major as we will couple the sensitive porous layer with an optical

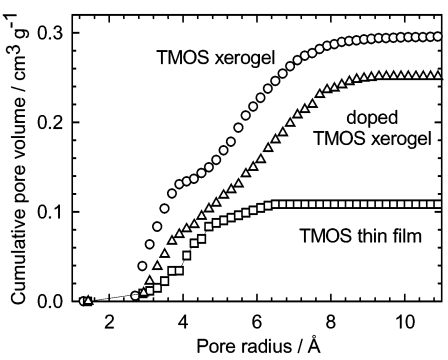

Fig. 6 Plot of the cumulative pore volume as a function of the hydraulic pore radius for a TMOS monolith, a TMOS monolith doped with pyranine ($5\ 10^{-5}$ M in the final sol) and a thin film analogue.

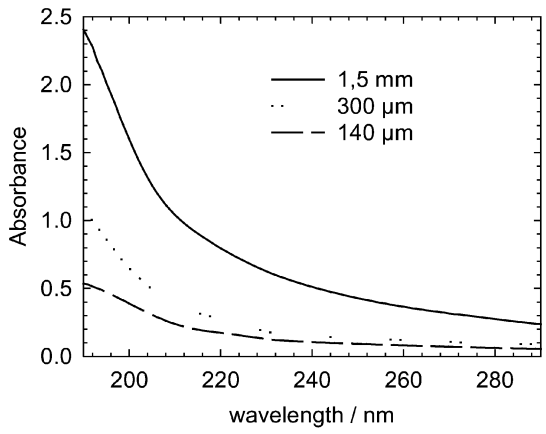

Fig. 7 Absorption spectra of the TMOS–MeTMOS 9 : 1 monoliths with different thickness.

transduction method. We demonstrated that it is possible to decrease the local polarity of the pores by increasing the proportion of MeTMOS in the hybrid matrices and thus to reduce the retention of water vapor, an important interfering gas of the atmosphere. We will show in a coming paper that, with the optimisation of the porosity, polarity and thickness of the xerogels, we will be able to detect benzene with a threshold of detection of 100 ppb.

Acknowledgement

Two of the authors, M.-L. Calvo-Muñoz and T.-H. Tran-Thi, acknowledge the financial support of the Conseil Général de l'Essonne and support from the EC Marie Curie training grant N° ERBFMBICT972340.

References

1 D. Avnir, D. Levy and R. Reisfeld, *J. Phys. Chem.*, 1984, **88**, 5956–5959.
2 B. Dunn and J. I. Zink, *J. Mater. Chem.*, 1991, **1**, 903–913.
3 D. Levy, S. Einnhorn and D. Avnir, *J. Non-Cryst. Solids*, 1989, **113**, 137–145.
4 J.-P. Boilot, J. Biteau, F. Chaput, T. Gagoin, A. Brun, B. Darracq, P. Georges and Y. Levy, *Pure Appl. Opt.*, 1998, **7**, 169–177.
5 *Chemistry, Spectroscopy and Applications of Sol–Gel Glasses. Structure and Bonding (77)*, eds. R. Reisfeld and C. K. Jorgensen, Springer-Verlag, Berlin, 1992.
6 C. Malins and B. D. Mac Craith, *Analyst*, 1998, **123**, 2373–2376.
7 J. Lin and C. W. Brown, *Trends Anal. Chem.*, 1997, **16**, 200–211.
8 B. C. Dave, B. Dunn, J. S. Valentine and J. I. Zink, *Anal. Chem.*, 1994, **66**, 1120a–1127a.
9 *Better Ceramics Through Chemistry VII: Organic/Inorganic Hybrid Materials*. eds B. K. Coltrain, C. Sanchez, D. W. Schaefer and G. L. Wilkes, Materials Research Society Publisher, Pittsburgh, PA, 1996.
10 H. Schmidt, *J. Non-Cryst. Solids*, 1985, **73**, 681–691.
11 M. Yamane, S. Inoue and A. Yasumori, *J. Non-Cryst. Solids*, 1984, **63**, 13–21.
12 J. J. van Beek, D. Seykens, J. B. H. Jansen and R. D. Schuiling, *J. Non Cryst. Solids*, 1991, **134**, 14–22.
13 F. Devreux, J.-P. Boilot and F. Chaput, *Phys. Rev. A*, 1990, **41**(12), 6901–6909.
14 M. J. van Bommel, T. N. M. Bernards and A. H. Boonstra, *J. Non-Cryst. Solids*, 1991, **128**, 231–242.
15 F. Brunet, *J. Non Cryst. Solids*, 1998, **231**, 58–77.
16 S. Brunauer, P. H. Emmett and E. Teller, *J. Am. Chem. Soc.*, 1938, **60**, 309–319.
17 S. Lowell and J. E. Shields, *Introduction to Powder Surface Area*, John Wiley & Sons, New York, 1984.
18 S. J. Gregg and K. S. W. Sing, *Adsorption, Surface Area and Porosity*, Academic Press, London, 1982.
19 A. Ayral, A. El Mansouri, M.-P. Vieira and C. Pilon, *J. Mater. Sci. Lett.*, 1998, **17**, 883–885.
20 J.-C. Pouxviel, J.-P. Boilot, J.-C. Beloeil and C. Lallemand, *J. Non Cryst. Solids*, 1987, **89**, 345–360.
21 J. Zarzycki, M. Prassas and J. Phalippou, *J. Mater. Sci.*, 1982, **17**, 3371–3379.
22 G. Engelhardt and D. Michel, *High Resolution Solid State NMR of Silicates and Zeolites*, Wiley, New York, 1987.
23 G. D. Sorarù, G. D'Andrea, R. Campostrini and F. Babonneau, *J. Mater. Chem.*, 1998, **5**(9), 1363–1374.
24 S. Diré, E. Pagani, F. Babonneau, R. Ceccato and G. Carturan, *J. Mater. Chem.*, 1997, **7**, 67–73.
25 Y. Yan, Y. Hoshino, Z. Duan, S. R. Chaudhuri and A. Sarkar, *Chem. Mater.*, 1997, **9**, 2583–2587.
26 L. Bois, PhD Thesis, 1993, Université de Paris VI, France.
27 R. A. Assink and B. D. Kay, *Mater. Res. Soc. Symp. Proc.*, 1984, **32**, 301–306.
28 C. J. Brinker, K. D. Keefer, D. W. Schaefer, R. A. Assink, B. D. Kay and C. S. Ashley, *J. Non-Cryst. Solids*, 1984, **63**, 45–59.
29 C. J. Brinker and G. W. Scherer, *Sol–Gel Science. The Physics and Chemistry of Sol–Gel Processing*, Academic Press, Boston, 1990.
30 T. M. Alam, R. A. Assink and D. A. Loy, *Chem. Mater.*, 1996, **8**, 2366–2374.
31 C. E. Bronnimann, R. C. Zeigler and G. E. Maciel, *J. Am. Chem. Soc.*, 1988, **110**, 2023–2026.
32 C. C. Liu and G. E. Maciel, *J. Am. Chem. Soc.*, 1996, **118**, 5103–5119.
33 B. Smith, *Infrared Spectral Interpretation : A Systematic Approach*, CRC Press, Boca Raton, 1999.
34 D. L. Wood, E. M. Rabinovich, D. W. Johnson, J. B MacChesney and E. M. Vogel, *J. Am. Ceram. Soc.*, 1983, **66**(10), 693–699.
35 A. L. Smith and D. R. Anderson, *Appl. Spectrosc.*, 1984, **38**(6), 822–833.
36 F. Orgaz and H. Rawson, *J. Non-Cryst. Solids*, 1986, **82**, 57–68.
37 J. H. Anderson and K. A. Wickersheim, *Surf. Sci.*, 1964, **2**, 252–260.
38 C. C. Perry and X. Li, in *Chemical and Processing of Advanced Materials*, ed. L. L. Hench and J. K. West, John Wiley & Sons, New York, 1992.
39 N. Barrash-Shiftan, B. B. Brauer and E. Pines, *J. Phys. Org. Chem.*, 1998, **11**, 743–750.
40 C. Prayer, PhD Thesis, 1997, Université de Paris XI, France.
41 V. R. Kaufman, D. Avnir, D. Pines-Rojanski and D. Huppert, *J. Non-Cryst. Solids*, 1988, **99**, 379–386.
42 N. Wittouck, E. De Schryver and I. Snijkers-Hendrickx, *J. Sol–Gel Sci. Technol.*, 1997, **8**, 895–899.
43 W. G. Fahrenholtz, D. M. Smith and D.-W. Hua, *J. Non-Cryst. Solids*, 1992, **144**, 45–52.
44 Y. Polevaya, J. Samuel, Michael Ottolenghi and D. Avnir, *J. Sol–Gel Sci. Technol.*, 1995, **5**, 65–70.
45 C. Krause, S. Klein, J. Kärger and W. F. Maier, *Adv. Mater.*, 1996, **8**, 912–916.
46 R. SH. Mikhail, S. Brunauer and E. E. Bodor, *J. Colloid Interface Sci.*, 1968, **26**, 45–53.